Nuclear motion captured by the slow electron velocity imaging technique in the tunnelling predissociation of the S1 methylamine

Doo-Sik Ahn, Jeongmook Lee, Young Choon Park, Yoon Sup Lee, and Sang Kyu Kim

Citation: J. Chem. Phys. **136**, 024306 (2012); doi: 10.1063/1.3675566
View online: http://dx.doi.org/10.1063/1.3675566
View Table of Contents: http://jcp.aip.org/resource/1/JCPSA6/v136/i2
Published by the American Institute of Physics.

Nuclear motion captured by the slow electron velocity imaging technique in the tunnelling predissociation of the S_1 methylamine

Doo-Sik Ahn,[a),b)] Jeongmook Lee,[a)] Young Choon Park, Yoon Sup Lee, and Sang Kyu Kim[c)]
Department of Chemistry, KAIST, Daejeon 305-701, South Korea

(Received 12 November 2011; accepted 13 December 2011; published online 9 January 2012)

Predissociation dynamics of methylamines (CH_3NH_2 and CH_3ND_2) on the first electronically excited states are studied using the slow-electron velocity imaging method to unravel the multi-dimensional nature of the N–H(D) chemical bond dissociation reaction which occurs via tunnelling. The nearly free internal rotation around the C–N bond axis is found to be strongly coupled to the reaction pathway, revealing nuclear motions actively involved in the tunnelling process on the S_1 potential energy surfaces. The vibrational state-resolved energy and angular distributions of photoelectron, ejected from the ionization mediated by the metastable intermediate S_1 state provide a unique way for mapping the predissociative potential energy surfaces. © *2012 American Institute of Physics*. [doi:10.1063/1.3675566]

I. INTRODUCTION

Chemical reactions often involve short-lived species, which play critical roles in the determination of many reaction outcomes such as quantum yields, reaction rates, or product state distributions. Time-resolved spectroscopic tools giving direct time scales of nuclear motions have been extremely useful for dynamic studies of such transient species. Frequency-domain spectroscopic studies, on the other hand, generally provide the static information of the molecular structure. However, there have been many cases where the frequency-domain spectroscopy is utilized in structural or dynamic studies of the transient species, if those are involved in the optical transition.[1–7] The negative ion photoelectron detachment spectroscopy pioneered by Neumark[8] was one of the most successful examples in this manner, giving the vibrational structure of the transition state in pre-designed bimolecular reactions. Along this line, the dispersed fluorescence spectroscopic study of CH_3I on the repulsive excited potential energy surface is quite notable since it reflects the structural change of the dissociating molecule, revealing the complicated nature of the reaction coordinate as well as the conical intersection configuration.[9] Two-color two-photon zero-electron kinetic energy spectroscopy, in which metastable intermediate states are involved in the $(1+1')$ ionization scheme, has also been employed for the same purpose as it provides sufficient energy resolution as well as high detection sensitivity.[10,11] All of frequency-domain spectroscopic methods are based on the validity of the Born-Oppenheimer approximation that the electronic transition is much faster than the nuclear motion, though a rather slow pumping process may diminish the transition probability for the system with short-lived intermediate state. Although only a few examples have been reported so far, the frequency-domain spectroscopy seems to be a quite powerful tool for the investigation of transient species, especially for grasping the multi-dimensional features of the potential energy surfaces.

The recently developed slow electron velocity map imaging (SEVI) method is very useful for the spectroscopic mapping of the potential energy surface as it reflects the electronic configuration as well as the vibrational structure of the predissociating molecule.[12,13] In SEVI, the first photon wavelength is fixed for the preparation of a single S_1 vibronic state whereas another tunable photon is used to ionize the molecule just above the vibrationally adiabatic ionization thresholds. The resulting photoelectron has the minimum kinetic energy while the energy resolving power ($\Delta E/E$) remains more or less same, giving much better energy resolution.[12,13] Because of this advantage, SEVI is being actively used in the investigation of the transition state of bimolecular reactions[14] or the intramolecular vibrational state redistribution process.[15] In this work, SEVI is employed for the study of predissociation dynamics of methylamines on the first electronically excited state. Energy and angular distributions of photoelectron from the ionization of predissociating molecule give the essential information about the complicated nature of the reaction path along which the chemical bond breaking event takes place via tunnelling. Tunnelling mechanism had been treated in the reduced dimensionality, and often assumed as a simple one-dimensional process in which the light atom caught in the well jumps to the outside of the barrier. Here, the nuclear motion associated with tunnelling on the multi-dimensional potential energy surface is captured in the SEVI spectrum.

Methylamine has been intensively studied as a good model system for spectroscopic and dynamic studies of predissociations.[16–25] It displays intriguing dynamical features such as a huge H/D isotope effect, indicating that the N–H(D) bond dissociation occurs via tunnelling at the zero-point level of S_1.[16–21] Predissociation dynamics is state

[a)] D.-S. Ahn and J. Lee contributed equally to this work.
[b)] Present address: Fritz-Haber-Institut der Max-Planck-Gesellschaft, Berlin, Germany.
[c)] Author to whom correspondence should be addressed. Electronic mail: sangkyukim@kaist.ac.kr.

dependent and the conical intersection seems to play an important role in the final product properties.[22] Even though product analyses reflect the exit dynamics, it is extremely hard to follow the trajectory back from the product to reactant for the irreversible chemical processes. Accordingly, for predissociation reactions where the initially prepared reactive flux is metastable, it may be desirable if one could figure out the shape of the potential energy surface along the reaction coordinate as the bond breakage is prompt once the flux escapes from the excited state potential well. In this sense, the (1+1′) SEVI using the S_1 intermediate state may provide the Franck-Condon mapping of the predissociative potential energy surface as the methylamine in the cationic ground state is stationary and bound, providing well-defined localized vibrational wave functions, which may serve as an effective basis set for describing S_1 states. The spectral pattern in SEVI should reflect the nature of the vibrational wave function of the predissociative S_1 state, and thereafter the shape of S_1 along the corresponding nuclear coordinate could be learnt. Angular distribution of photoelectron gives the electronic configuration character of the Ã state, which may vary with the nuclear displacement along the reaction coordinate especially since the extent of coupling between two electronically excited states depends on the nuclear configuration due to the nearby existence of the conical intersection.

II. EXPERIMENTAL

The experimental setup was given in detail previously.[22] In brief, the high purity CH_3NH_2 (Aldrich) sample was diluted with the Ne carrier gas (~3%) to prevent contributions from methylamine clusters. The CH_3ND_2 sample was prepared by the H/D exchange between CH_3NH_2 and excess D_2O, followed by the dehydration using the solid KOH. The gas mixture was expanded into vacuum through a 0.3 mm diameter nozzle (Parker, General Valve series 9), and skimmed through a 0.5 mm diameter skimmer (Beam Dynamics). The backing pressure of the gas mixture was ~2 atm. The third harmonic output of the neodymium-doped yttrium aluminum garnet (Nd:YAG) laser (Spectra-Physics, GCR-150) was used to pump the dye laser (Lamda-Physik, Scanmate II) in order to generate the laser pulse in the 234–240 nm range for the excitation of methylamines. The ionization laser in the 285–320 nm region was generated by frequency doubling of the dye laser output (Lumonics, Spectrummaster) pumped by the second harmonic output of another Nd:YAG laser (Continuum, Surelite). Two output lasers were synchronized with the opening of nozzle (10 Hz) and counterpropagated to be focused by 250 mm focal length lens onto the molecular beam. The polarizations of two laser beams were perpendicular to the time-of-flight axis and parallel to the detector. One-color (1+1) ionization scheme was used for conventional photoelectron imaging, while a two-color (1+1') scheme was used for the SEVI. Velocity mapping of photoelectron images were obtained by position sensitive detector (Burle) coupled with a personal computer-interfaced CCD camera system. The event counting and centroiding were carried out by the MEGAPIXEL software.[26] The SEVI images were taken at the low electric field condition (45.7 V/cm), and reconstructed using the BASEX program.[27] The photoelectron angular distribution was fit with Legendre polynomials up to the 4th order. The typical energy resolution of SEVI is estimated to be around 20 cm^{-1}, which is much improved than 400 cm^{-1} of the conventional velocity map images in the present experimental condition. Numerical optimizations with the equation-of-motion coupled cluster singles and doubles (EOM-CCSD) method/6-31+G(*d,p*) level of theory were carried out to get minimum geometry and transition state in the S_1 state using the GAUSSIAN 09 program suit.[28]

III. RESULTS AND DISCUSSION

Photoelectron spectra by the one-color two-photon (1+1) ionization velocity map imaging (R2PI-VMI) technique, taken via ν_9 ($NH(D)_2$ wagging) = 1 states of the Ã CH_3NH_2 and CH_3ND_2 (+636 and +487 cm^{-1} above each S_1 origin, respectively) are shown in Fig. 1. Even though the laser pulse duration of 5 ns is long enough for the further excitation of radical products, the laser intensity is much reduced to exclude the possibility of multi-photon processes. In Fig. 1(a), the largest kinetic energy peak corresponds to the $\nu_9^+ = 1$ level of the ground $CH_3NH_2^+$, whereas the progression bands added on $\nu_9^+ = 1$ are clearly seen with an interval of ~3400 cm^{-1}. Another progression placed on the $\nu_9^+ + \nu_4^+$ (NH_2 scissor) combination band is also weakly observed. The same pattern of progression bands is observed in the photoelectron spectrum of CH_3ND_2 with a much redshifted interval of ~2300 cm^{-1} in Fig. 1(b). The large frequency shift due to the NH_2/ND_2 substitution indicates that these prominent progression bands are due to the N–$H(D)_2$ symmetric stretching vibrational mode (ν_1^+). Observation of the long progression bands of the N–$H(D)_2$ stretching mode then suggests that the predissociative Ã states of methylamines are quite anharmonic along the N–H(D) elongation coordinate, as expected in previous studies.[17] The intensity distributions of the ν_1^+ progression bands could be explained only by introducing the anharmonicity of the S_1 state potential energy surface along the N–H(D) elongation coordinate (*vide infra*), which originates from the coupling of the optically bright 3*s* bound state with the optically dark repulsive $n\sigma^*$ state at the molecular geometry with somewhat elongated N–H(D) bond lengths. It should be noted that the photoelectron spectrum taken via one quantum of NH_2 wagging mode (ν_9) of the intermediate Ã state gives rise to the identical spectrum with the one taken via the S_1 origin except the corresponding energetic shift, showing that the excitation of ν_9 is conserved in the ionization process.

Two-colour two-photon (1+1′) SEVI spectra, compared with the (1+1) R2PI-VMI spectra, show much enhanced energy resolution, revealing the more precise energy spacing as well as distinct spectral features (Fig. 1). One can now not only locate the more precise positions of $NH(D)_2$ symmetric stretching bands but also identify $NH(D)_2$ anti-symmetric stretching bands, which are located at slightly higher energy positions than their respective symmetric stretching modes, giving 3310 (2396) and 3415 (2556) cm^{-1} for $NH_2(ND_2)$ symmetric or anti-symmetric stretching (ν_{10}^+) modes of $CH_3NH_2^+$ ($CH_3ND_2^+$), respectively (Figs. 1 and 2). The fact

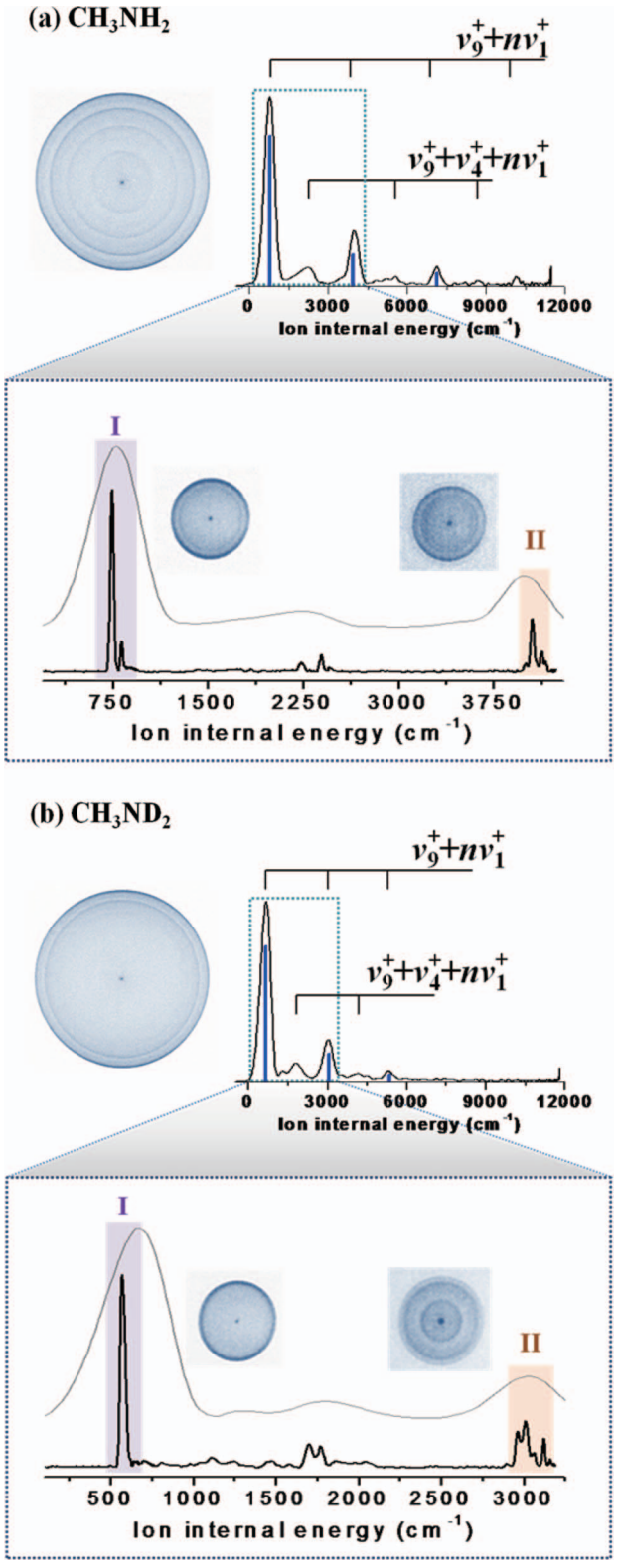

FIG. 1. One-color two-photon (1+1) ionization velocity map photoelectron images with reconstructed photoelectron spectra (upper parts), and two-color two-photon (1+1′) ionization SEVI images with corresponding photoelectron spectra (lower parts) of (a) CH_3NH_2 and (b) CH_3ND_2 taken via the $S_1(\nu_9 = 1)$ intermediate state, respectively. The blue stick spectra represent the Frank-Condon simulation (see the text). Here ν_1^+, ν_4^+, and ν^+_9 are $NH(D)_2$ symmetric stretching, scissoring, or wagging mode of the methylamine cation, respectively. In photoelectron images, the ring with the smaller radius corresponds to the peak with the higher ion internal energy in photoelectron spectra. The regions I and II represent the energy regions near ν_9^+ and $\nu_9^+ + \nu_1^+$ modes, respectively.

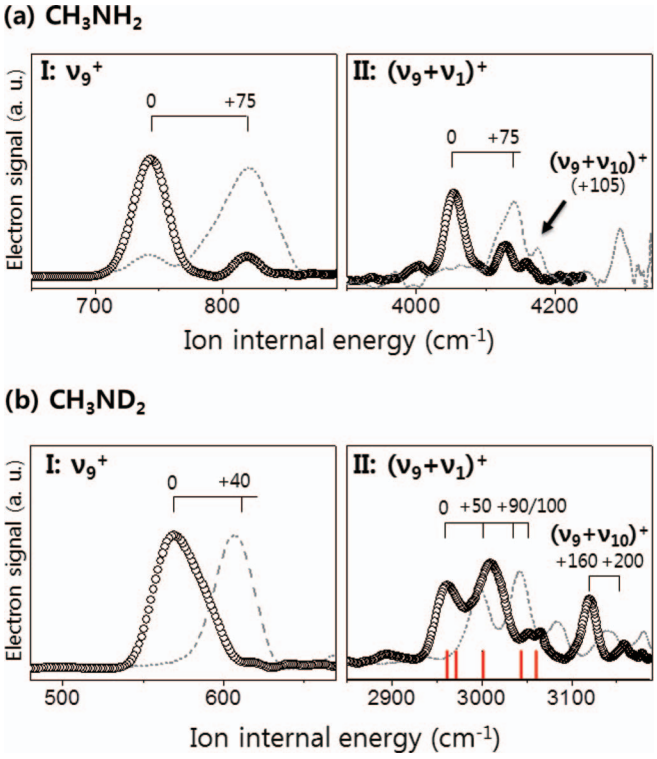

FIG. 2. Regions I and II of SEVI spectra of (a) CH_3NH_2 and (b) CH_3ND_2 indicated in Fig. 1. Open circles via the $\nu_9 = 1$ with no torsional excitation, dashed lines via the ν_9 combined with torsional mode excitation of the S_1 state. Here, ν_1^+, ν_9^+, and ν_{10}^+ are $NH(D)_2$ symmetric stretching, wagging, or anti-symmetric stretching mode of the methylamine cation, respectively. The $(\nu_9 + \nu_{10})^+$ combination bands are observed at 105 or 160 cm^{-1} higher than $(\nu_9 + \nu_1)^+$ bands of CH_3NH_2 or CH_3ND_2, respectively. In region II of (b) CH_3ND_2, a simulated spectrum (red sticks) calculated from the hindered rotor Hamiltonian[17] is shown. In order of increasing ion internal energy, red sticks correspond to rotational transitions of $0a_1 \leftarrow 0a_1$, $1e \leftarrow 1e$, $2e \leftarrow 1e$, $3a_1 \leftarrow 0a_1$, and $3a_2 \leftarrow 0a_1$.

that symmetry-forbidden $NH(D)_2$ anti-symmetric bands are weakly observed suggests that the reactive flux on the $\tilde{A}$ state may explore the phase space spanned over the anti-symmetric stretching coordinate. This could be rationalized by the H(D) atom dissociation coordinate on the S_1 state. The asymmetric breakdown of two identical N–H(D) bond lengths should be prior to the N–H(D) bond dissociation along the repulsive $n\sigma^*$ state, and it gives the Frank-Condon intensity to $NH(D)_2$ anti-symmetric stretching on the cationic state. It should be noted that the amino anti-symmetric stretching band is more strongly observed in CH_3ND_2 compared to that in CH_3NH_2 (Fig. 2), and the slower tunnelling reaction of the former may be responsible for this observation as the retention time of the CH_3NH_2 reactive flux may be too short to be probed in the rather slow ionization process in this work.

The more dramatic spectral feature is found in the excitation of the hindered rotor states in SEVI spectra, which is very different for two isotopologues and strongly dependent on the combined vibrational bands. The excitation of bands due to internal rotational motion around the C–N bond axis is observed as distinct peaks in SEVI spectra in Figs. 1 and 2. For CH_3NH_2, for both the ν_9^+ (region I) and $\nu_1^+ + \nu_9^+$ (region II) bands, the internal rotor state excitation is only weakly observed with an apparent interval of 75 cm^{-1}. For

CH_3ND_2, however, the internal rotor excitation is found to be quite significant in the region II, whereas it is not in the region I (Fig. 2). The positions of internal rotation are energetically well matched with calculated energy levels based on the hindered rotation Hamiltonian[17] (Fig. 2(b)).

To identify the effect of torsional excitation on the S_1 to SEVI spectrum, we carried out another experiment at different excitation energies, which control internal rotational levels of S_1. In Fig. 2(a), for CH_3NH_2, the ionization via the excited torsional mode in the S_1 state gives rise to the enhancement of the photoelectron signal associated with the corresponding torsional mode of the cation in the SEVI spectrum, and this is in accord with the propensity rule. This is consistent for both regions I and II. In the region II, the main peak was shifted like in the region I while a peak for anti-symmetric stretching stayed on the less shifted position. This also applies to the case of CH_3ND_2 in the region I. The apparent energy interval is found to be red shifted to 40 or 50 cm^{-1} for CH_3ND_2 in the regions I and II, respectively. These spectroscopic features are quite normal if the ionization process does not induce any other torsional excitation. This propensity rule is always valid in the wide range of torsional state of S_1. The main peak is always shifted by the amount of extra-excitation energy. For the region II of CH_3ND_2, however, the highly excited torsional bands are observed and those are apparently shifted by the amount of extra energy given in the first excitation without a significant change of whole profile. This may suggest that torsional levels defined at the minimum potential energy surface do not exactly match with those manifested at the edge of the potential energy surface along the N–D elongation coordinate. It should also be noted that the spectroscopic features regarding the torsional rotor is quite complicated[17] due to its strong coupling to the overall rotational operator. The red stick spectrum shown in Fig. 2(b) represents transitions between torsional energy levels, calculated with a Hamiltonian used in Ref. 17. Our SEVI resolution is not high enough for the full spectroscopic analysis. Even prior to full analysis, however, it is quite interesting to observe the mode-selective torsional excitation in the ionization process as it may represent the nature of the reaction pathway at the exit region of the reaction barrier, reflecting the nuclear motion involved in tunnelling which is comprised of multiple internal coordinates.

One of the fundamental questions in tunnelling would be how atoms move especially along the vibrational degrees of freedom other than one-dimensional coordinate along which the light atom escapes from the well. Our observation may give an answer for such an intriguing question for the case of the methylamine predissociation. The H-atom tunnelling at the zero-point level of the S_1 methylamine is very fast, giving broad absorption features from which the lifetime had been estimated to be less than 300 fs.[17] Thus, the ultrafast H-atom tunnelling of CH_3NH_2 may occur in the effectively frozen molecular geometry. In CH_3ND_2, however, the tunnelling rate is greatly reduced to give the lifetime of a few ps.[17] In this case, the D-atom tunnelling may be accompanied by the nuclear motion relevant to the reaction pathway. The fact that the internal rotor excitation of SEVI is significant only in the region II of CH_3ND_2, thus indicates that the internal rotation is strongly involved in the tunnelling reaction pathway especially at the exit region of the potential energy surface where the N–D bond is somewhat elongated. Classically, one can imagine that as the N–D bond stretches to hit the barrier, the torsional motion is being activated so that tunnelling process becomes more efficient. The high level *ab initio* calculation is useful to support such a plausible explanation. The S_1 potential energy surface, calculated at the EOM-CCSD level as a function of two N–H bond lengths with other geometrical parameters frozen is shown in Fig. 3. The potential energy surface is quite anharmonic, and the Franck-Condon calculation based on the associated eigenstates reproduces the experiment very well in terms of the intensity distribution of the ν_1^+ progressions (blue sticks in Fig. 1). Moreover, the fully optimized transition structure using our EOM-CCSD calculation gives the ciscoid structure on the reaction barrier top (Fig. 3). It suggests that the torsional activation about the C–N bond may facilitate the tunnelling process since it will lower the effective tunnelling barrier. In other words, the torsional motion about the C–N bond is activated whenever the reactive flux bound in the well is looking for the minimum energy path along the tunnelling reaction coordinate. In fact, the planar structure is not a minimum when two N–H(D) bonds are not identical like transition state. In other words, sixfold potential at the minimum structure of S_1 along C–N torsional coordinate is gradually changed to threefold potential at transition state, even though the rotational barrier is still quite small. This correlated change of C–N rotation along dissociation coordinate is important to determine the energy level of internal states as well as Frank-Condon intensities between internal rotation states because of the displacement of PES for C–N rotation. Classically, this means that C–N rotation can be enforced by topological change of S_1 PES along N–H(D) dissociation coordinate since both coordinates are strongly coupled with a static PES manner. The more flux near transition state (or far from minimum) of CH_3ND_2 due to the less efficient tunnelling can lead to more torsional excitation, and is reflected on the ND_2 stretching accompanied torsional excitation and observation of non-allowed ND_2 anti-symmetric stretching vibration which can reflect more elongated region toward transition state. Unfortunately, we failed to obtain a reliable SEVI spectrum at the $\nu_9^+ + 2\nu_1^+$ or $\nu_9^+ + 3\nu_1^+$, which could be quite helpful for the further spectral confirmation, due to the small intensity.

Angular distributions of photoelectrons are dependent on the associated cationic vibrational states. The anisotropy parameter (β_2) of the photoelectron from CH_3NH_2 is estimated to be 0.6 ± 0.1 for the photoelectron associated with ν_9^+ (region I), whereas it is decreased to 0.3 ± 0.1 for that associated with the $\nu_1^+ + \nu_9^+$ (region II) bands, indicating that the electronic configuration varies with the change of the nuclear configuration on the single adiabatic potential energy surface. The decrease of β_2 for the $\nu_1^+ + \nu_9^+$ band indicates that the electronic configuration becomes less Rydberg-like at the exit edge of the potential well. This experimental finding makes sense at least qualitatively, as the S_1 state barrier should originate from avoided crossing of the 3*s* Rydberg bound and the repulsive $n\sigma^*$ states. As the Franck-Condon

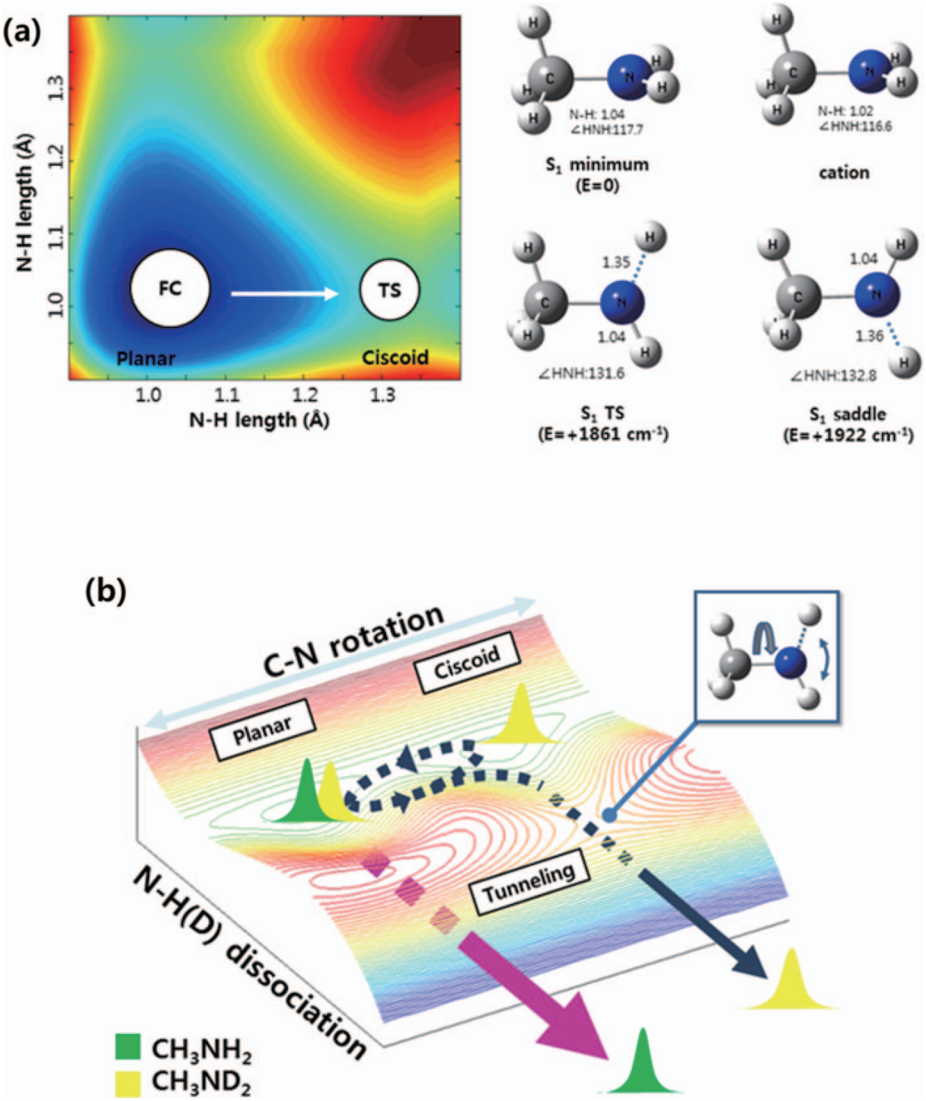

FIG. 3. (a) Schematic of the calculated potential energy surfaces of the S_1 state along two N–H bond elongation coordinates, shown with optimized geometries at the minimum energy point and transition state. (b) Proposed mechanism for tunnelling reactions of CH_3NH_2 and CH_3ND_2 on the S_1 states. The ultrafast H-atom tunnelling occurs at the frozen geometry whereas the D-atom tunnelling takes place with the significant torsional mode excitation during its longer retention time.

window of the ionization moves toward the exit region, the electronic character of $n\sigma^*$ contributes more significantly, resulting in the decrease of the anisotropy parameter which otherwise would remain high due to the *p*-partial wavelike character of the photoelectron from the 3*s* Rydberg state. The general trend of β_2 is found to be same for CH_3ND_2. The detailed quantitative anisotropy data, however, are quite complicated, and the more elaborate theoretical calculations would be necessary for the further analysis.

Tunnelling is a quantum-mechanical process for which the multi-dimensional character is hardly understood yet. When the tunnelling rate is slow enough to be comparable to the time scale of relevant vibrational oscillations, it may be possible to probe key vibrational modes, which are strongly coupled to the reaction coordinate. For the S_1 methylamine, the nearly freely rotating internal rotor is strongly coupled to the tunnelling reaction pathway. It is also demonstrated that SEVI could be a promising tool for the investigation of the multi-dimensional potential energy surfaces. The highly resolved photoelectron spectrum taken via the short-lived intermediate states provides the slice-mapping of the potential energy surfaces according to the Franck-Condon overlap of the metastable state with well-defined quantum state wave functions of the ground state cation.

ACKNOWLEDGMENTS

This work was supported by National Research Foundation (NRF-2011-0016447, 2010-0000068 & 313-2008-2-C00401). The support from the Center for Space-Time Molecular Dynamics (2011-0001216) is also appreciated.

[1]K. Müller-Dethlefs and E. W. Schlag, Angew. Chem., Int. Ed. **37**, 1346 (1998).
[2]F. Merkt and H. J. Wörner, Angew. Chem., Int. Ed. **48**, 6404 (2009).
[3]S. A. Asher, Annu. Rev. Phys. Chem. **39**, 537 (1988).
[4]J. S. Lim and S. K. Kim, Nat. Chem. **2**, 627 (2010).
[5]D.-S. Ahn, S. Y. Kim, G.-I. Lim, S. Lee, Y. S. Choi, and S. K. Kim, Angew. Chem., Int. Ed. **49**, 1244 (2010).

[6]J. S. Lim, Y. S. Lee, and S. K. Kim, Angew. Chem., Int. Ed. **47**, 1853 (2008).
[7]J. S. Lim, I. S. Lim, K.-S. Lee, D.-S. Ahn, Y. S. Lee, and S. K. Kim, Angew. Chem., Int. Ed. **45**, 6290 (2006).
[8]D. M. Neumark, Acc. Chem. Res. **26**, 33 (1993).
[9]M. O. Hale, G. E. Galica, S. G. Glogover, and J. L. Kinsey, J. Phys. Chem. **90**, 4997 (1986).
[10]I. Fischer, A. Lochschmidt, K. Müller-Dethlefs, and V. E. Bondybey, J. Phys. Chem. **98**, 2024 (1994).
[11]B. Urban and V. E. Bondybey, Phys. Chem. Chem. Phys. **3**, 1942 (2001).
[12]C. Nicole, I. Sluimer, F. Rosca-Pruna, M. Warntjes, M. Vrakking, C. Bordas, F. Texier, and F. Robicheaux, Phys. Rev. Lett. **85**, 4024 (2000).
[13]D. M. Neumark, J. Phys. Chem. A **112**, 13287 (2008).
[14]E. Garand, J. Zhou, D. E. Manolopoulos, M. H. Alexander, and D. M. Neumark, Science **319**, 72 (2008).
[15]K. L. Reid, Int. Rev. Phys. Chem. **27**, 607 (2008).
[16]S. J. Baek, K.-W. Choi, Y. S. Choi, and S. K. Kim, J. Chem. Phys. **117**, 10057 (2002).
[17]S. J. Baek, K.-W. Choi, Y. S. Choi, and S. K. Kim, J. Chem. Phys. **118**, 11026 (2003).
[18]S. J. Baek, K.-W. Choi, Y. S. Choi, and S. K. Kim, J. Chem. Phys. **118**, 11040 (2003).
[19]M. H. Park, K.-W. Choi, Y. S. Choi, and S. K. Kim, J. Chem. Phys. **125**, 084311 (2006).
[20]R. Marom, C. Levi, T. Weiss, S. Rosenwaks, Y. Zeiri, R. Kosloff, and I. Bar, J. Phys. Chem. A **114**, 9623 (2010).
[21]C. Levi, R. Kosloff, Y. Zeiri, and I. Bar, J. Chem. Phys. **131**, 064302 (2009).
[22]D.-S. Ahn, J. Lee, J.-M. Choi, K.-S. Lee, S. J. Baek, K. Lee, K.-K. Baeck, and S. K. Kim, J. Chem. Phys. **128**, 224305 (2008).
[23]A. Golan, S. Rosenwaks, and I. Bar, J. Chem. Phys. **125**, 151103 (2006).
[24]G. C. G. Waschewsky, D. C. Kitchen, P. W. Browning, and L. J. Butler, J. Phys. Chem. **99**, 2635 (1995).
[25]C. L. Reed, M. Kono, and M. N. R. Ashfold, J. Chem. Soc., Faraday Trans. **92**, 4897 (1996).
[26]W. Li, S. D. Chambreau, S. A. Lahankar, and A. G. Suits, Rev. Sci. Instrum. **76**, 063106 (2005).
[27]V. Dribinski, A. Ossadtchi, V. A. Mandelshtam, and H. Reisler, Rev. Sci. Instrum. **73**, 2634 (2002).
[28]M. J. Frisch, G. W. Trucks, H. B. Schlegel *et al.*, GAUSSIAN 09, Revision A.1, Gaussian, Inc., Wallingford, CT, 2009.